Spectroscopic analysis of hot emission-line stars using the medium resolution survey of LAMOST DR6

MAHIGUHAPPRIYAPRAKASH

Shaheed Rajguru College of Applied Sciences for Women,
University of Delhi, Delhi

DR. BLESSON MATHEW

Assistant Professor,
CHRIST (Deemed to be University), Bengaluru

April-June 2021

CERTIFICATE

This is certify that the project report entitled "SPECTROSCOPIC ANALYSIS OF HOT EMISSION-LINE STARS USING THE MEDIUM RESOLUTION SURVEY OF LAMOST DR6", is a record of bonafide work carried out by MAHIGUHAPPRIYAPRAKASH under my supervision and guidance in the fulfilment of the requirement for the Summer Research Fellowship offered by Indian Academy of Sciences, Bengaluru under SRFP 2021.

Dr. BLESSON MATHEW
Assistant Professor,
CHRIST (Deemed to be University), Bengaluru.

August 2021
Bengaluru

DECLARATION

I MAHIGUHAPPRIYAPRAKASH, hereby, declare that the project report entitled "SPECTROSCOPIC ANALYSIS OF HOT EMISSION-LINE STARS USING THE MEDIUM RESOLUTION SURVEY OF LAMOST DR6" is based on the innocent work done by me during the course of Summer Research Fellowship Programme 2021, at CHRIST (Deemed to be University), Bengaluru. The work presented in this project report hasn't been submitted for the award of any other degree or diploma elsewhere.

MAHIGUHAPPRIYAPRAKASH

11/08/2021

Erode

ACKNOWLEDGEMENTS

I would like to express my sincere gratitude and deepest appreciation to all who made it possible for me to complete this project. My heartfelt gratitude to Indian Academy of Sciences, Bengaluru for giving me the opportunity to work as a Summer Research Fellow under SRFP 2021. I would like to thank my supervisor Dr. Blesson Mathew, Assistant Professor, CHRIST (Deemed to be University), Bengaluru for his patience, guidance and timely suggestions during the entire tenure of the project. I would like to express my gratitude towards my co-supervisor Mr. Shridharan B, CHRIST (Deemed to be University), Bengaluru whom I frequently contacted for any queries regarding my work for his kind co-operation and encouragement which helped me in completion of this project. I would like to acknowledge the efforts of Ms. Anusha R, Project Assistant, CHRIST (Deemed to be University), Bengaluru for being attentitve to the minute details in the project and supporting in the successful completion of the project work.

My sincere thanks to Dr. Alka Vohra Kuanr, Associate Professor & Teacher in Charge, Department of Physics, Shaheed Rajguru College of Applied Sciences for Women, University of Delhi, Delhi for being a constant source encouragement and having belief in me. I would like to acknowledge Dr. Kishan Das, Dr. Rashmi Verma and Dr. Rajan Goyal, Faculty members, Shaheed Rajguru College of Applied Sciences for Women, University of Delhi, Delhi who guided me through the process of applying for the summer research fellowship and for their willingness to refer me for the same. Without their passionate participation and input, my work could not have been successfully conducted. A speical thanks to all my friends who helped me out with their abilities and being there for me during the toughest times. My sincere thanks to my parents who support me with all my decisions and motivate me to give my best in anything I pursue. This accomplishment would not have been possible without them. Thank you all.

MAHIGUHAPPRIYAPRAKASH

Contents

Abstract

Hot emission-line stars such as Oe, Be and Ae type stars are found to be in the top of the main sequence in the Hertzsprung-Russell Diagram, with temperatures ranging from 7,500 K to over 25,000 K and color varying from blue to blue-white. They show prominent emission lines due to the presence of gaseous circumstellar disk around them. The strength of Balmer lines decrease from O- to A- type stars in which Hα is commonly observed. The spectral lines observed in these stars show effects of Doppler broadening, which happens due to the Doppler shift in the atoms present in the gaseous disk. Shridharan et al. (under review) analyzed the archival spectra of hot stars (OBA) from LAMOST data release 5 and identified 3339 hot emission-line stars and classified into various categories. Upon comparing these stars with LAMOST data release 6, around 85 stars were found to have medium resolution spectra available, which could aid in analysing some of the inherent line properties in the spectrum. For this study, the projected rotational velocities (vsin$i$) of 30 out of 85 samples from the list have been calculated using the Doppler broadening effect observed in Hα profile of that object using python code and compared. Out of the samples observed, Be type stars tend to show largest value of 'vsin$i$' which suggests that Be type stars rotate the fastest amongst other hot emission-line stars.

1 Introduction

Astronomical spectroscopy is the study of components of the electromagnetic radiation from a stellar object, particularly in the visible region, which helps in inferring physical properties of that object. The continuous spectrum of electromagnetic radiation which comes out of a prism is expected from stars as well, but instead we end up getting a spectrum with dark lines on a bright background or bright lines on dark background on the continuous spectrum. This is because the light emitted from the stars first passes through the outermost stellar layer, called the photosphere that absorbs radiation at particular wavelength. Stars normally show absorption spectra but some exceptions show emission profile in their spectra as well. One of the reasons is due to the presence of gaseous circumstellar disk around them. A stellar spectrum is normally characterised by a continuum peak (black-body continuum spectrum), absorption lines and noise.

1.1 Classification of Stars

According to the Harvard Classification Scheme, stars are classified as O, B, A, F, G, K, M, L and T, where O, B, A are hot stars whose temperature varies from 7,500 K to over 25,000 K and normally blue to blue-white in color.

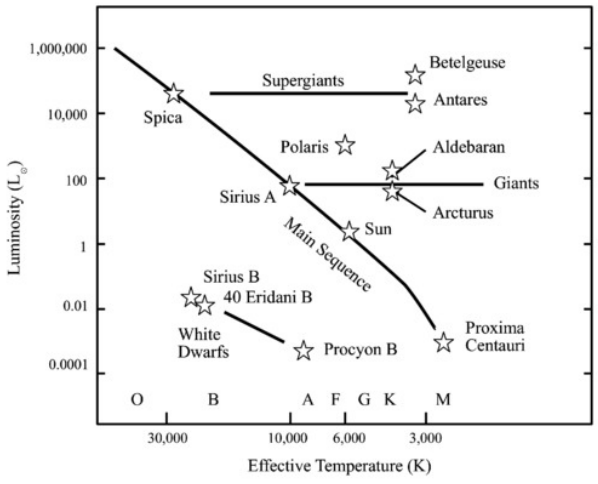

Figure 1: H-R Diagram. *Source: NASA*

The stellar classification plotted against other physical properties like temperature, absolute magnitude and luminosity are illustrated in Hertzsprung-Russell Diagram, which is commonly known as H-R Diagram (Figure 1). There are 3 main regions in H-R diagram that shows the evolutionary stage of stars. The first region is the *Main Sequence* where the star spends most of its lifetime burning Hydrogen to Helium in its core. The second region consists of Red Giants, when the star runs out of Hydrogen and starts using Helium and other heavy elements from Carbon, Nitrogen, Oxygen to Iron. Massive stars undergo supernova explosion after this stage. The remains of the core becomes a highly dense neutron star. The stars that exhibit emission lines in their spectra, especially Hα, are denoted by 'e' after their classification. Some significant examples are Oe, Ae and Be type stars. Distinctive forbidden neutral and low ionisation emission line are observed in spectra of some stars which are allowed if approximations associated with the formation of the line is not made. These stars are denoted by '[e]' after their classification. Some significant examples are A[e] and B[e] type stars.

1.2 Balmer Lines

When the excited electron in the unstable atomic level n = 3 of a Hydrogen atom transits to more stable atomic level n = 2, a strong red line is observed in the spectrum which corresponds to wavelength of $\lambda = 6562.8$ Å and it is the first transition in the Balmer Series. Hα line is observed in spectra of almost all stellar objects due to the abundance of Hydrogen in the Universe. It is mostly seen as an absorption line in stars and as emission line in AGNs and planetary nebulae.

1.3 Stellar Rotation

The axes of stars observed from the earth are seemingly inclined to the line of sight that connects the star and earth. The observer tends to find the rotational velocity of that star to be the projected velocity rather than the original equatorial rotational velocity 'v'. This projected rotational velocity 'vsin$i$' can be calculated from the spectra that we get from the star using Doppler broadening method as the spectral lines suffer Doppler effect due to relative motion of the object with respect to the observer. This causes the spectral line to look like a Gaussian-profile.

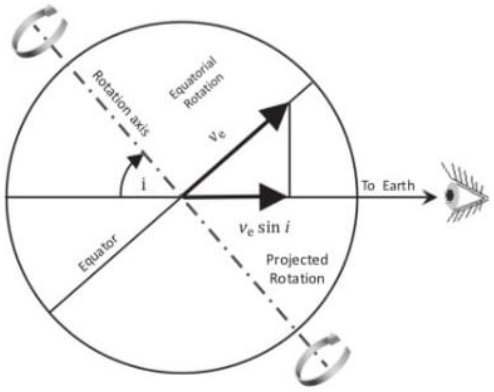

Figure 2: Stellar Rotation. *Source: Cambridge University Press*

The profile obtained due to Doppler broadening is known as a Doppler profile. Using Doppler broadening technique, 'vsin$i$' can be calculated by determining the Doppler width of the profile and multiplying it with the speed of light. Figure 2 shows the shows the relation of velocity components of a star as a function of the inclination angle i between the line of sight to Earth and the rotation axis.

$$vsini = \frac{\Delta\lambda}{\lambda} \times c \tag{1}$$

where $\Delta\lambda$ is the Doppler width, λ is the wavelength of light originally emitted by the source and c is the speed of light.

2 Data

Large Sky Area Multi Object Fibre Spectroscopic Telescope, commonly known as LAMOST, is a meridian reflecting Schmidt telescope that has wide field of view with limited aberration. It consists of 4000 optical fibres that are capable of capturing 4000 objects in one instance. The spectral range varies from 3700 - 9000 Å. The range of observable sky varies from -10° to $+90^\circ$ declination.

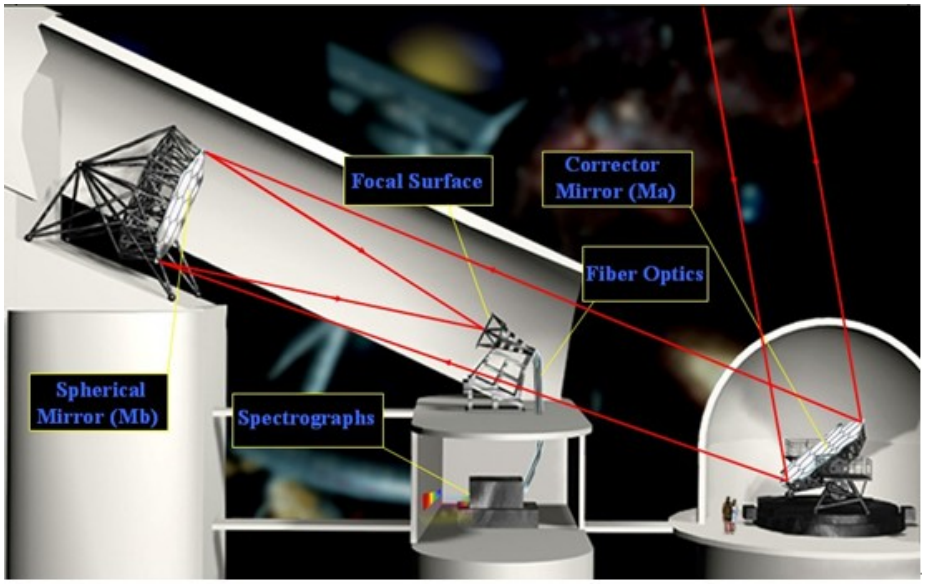

Figure 2 LAMOST overview

Figure 3: LAMOST setup. *Source:* LAMOST

Volume Phase Holographic Gratings are used and the spectral resolution can be 1000 or 5000 depending on the use of gratings and camera positions. Light from the source first strikes the corrected mirror *Ma* and then directed to the spherical mirror *Mb* to focus it on the focal surface. This is then sent through the optical fibres to the spectrograph where the spectrum is obtained. This spectroscopic data obtained from the spectrograph is stored as FITS file made available for public use in the official website of each data release. The overview of this setup is shown below. Figure 3 shows the cross sectional view of the LAMOST setup.

2.1 Low Resolution Survey Program from LAMOST

LAMOST consists of 16 spectrographs that supports low spectral resolution of R $\sim$ 1800 and can accomodate 250 fibres. These spectrographs are capable of obtaining spectra of 4000 celestial objects simultaneously via fibres of 3.3$''$ located in 5° field of view of the telescope. The wavelength range of each spectrograph is from 3700 Å to 9000 Å and spectral resolution can be either 1000 or 5000 depending on the gratings used and camera positions. The data release 6 of low resolution survey include stellar spectra, galaxy spectra, quasar spectra and unknown object spectra, each of them wavelength calibrated. The name of the FITS file is of the form *spec-MMMMM-YYYY_spXX-FFF.fits* where *MMMMM*, *YYYY*, *XX* and *FF* represent the local modified Julian day, the plan identity string, the spectroscopic identity number which is between 1 and 16, and the fiber identity number which is in the range of 1 to 250. The FITS file consists of a primary header data (HDU), an optional conforming extension and other optional spectral records.

2.2 Medium Resolution Survey Program from LAMOST

The spectrographs in LAMOST support medium spectral resolution of R $\sim$ 7200. In Medium Resolution mode, the blue cameras cover wavelength range from 4950 Å to 5350 Å and the red cameras cover from 6300 Å to 6800 Å which is not as large as the low resolution spectra. With MRS, the rotation of the stars can be well estimated with comparatively less uncertainty than LRS. The coverage of wavelength in medium resolution survey enables to measure about 20 elemental abundances and the red part of the spectra covers Hα, [NII] and [SII] emission lines effectively, which is crucial for sciences related to planetary nebulae, supernova remnants, galactic nebulae etc. The Hα profile is essential for study of proto-planetary disk surrounding young stars.

The mid-resolution spectral data from LAMOST DR6 is in the form of multidimensional FITS file that consists of the following details: spectrum, inverse variance for flux, continuum subtracted flux, and-mask array, or-mask array (or) pixmask. We can get two spectra within an exposure of every target including a blue (B) and a red (R) band whose wavelength ranges are 4950 Å - 5350 Å and 6300 Å - 6800 Å respectively. The coadded B and R band spectra is obtained by combing the single exposure spectra after the object is observed several times. The spectral data in the form of FITS file is obtained from archival database of LAMOST. The FITS files of

MRS in the format *med-MMMMM-YYYY_spXX-FFF.fits*. The FITS file of a target will have m (m_i=n) B band and t (t_i=n) R band single exposure spectra if it has n times exposures. If at least one of m and t is equal to zero, no coadded spectrum is provided in the FITS file. The LAMOST MRS FITS file has extension 0 as its primary HDU, which is not followed by a primary data array, and extension 1 and 2 restore the coadded B and R band spectra respectively. From extensions 3 to m+2, the information of m B band spectra obtained within n exposures is stored while from extensions m+3 to m+t+2, the information of t R band spectra obtained in n exposures is stored.

The analysis is performed by first normalizing the data obtained from LAMOST and make the continuum level to unity so that we can nullify the effect of the grating blaze and change in detector sensitivity over the wavelength region observed. The next step is to calculate the Equivalent Width (EW) and Full Width at Half-Maximum (FWHM) values of the Hα profile of the spectra. Then using Doppler broadening, the projected velocities of star samples are estimated.

3 Analysis

3.1 Data Extraction

The aim of this project is to determine and compare the projected velocities of 85 out of 3339 hot emission-line stars analysed by Shridharan et al. (under review) using LAMOST DR5. These 85 stars have medium resolution spectra available in LAMOST DR6. We analyzed their Hα profiles and checked which type of stars rotate the fastest.

Stars with bright emission lines in their spectrum that show Balmer emission along with metallic emission lines are generally known as Emission-line stars (ELS). The emission lines are formed due to recombination process happening in the circumstellar disk region. ELS can be classified into different categories based on the evolutionary stage, spectra type and mass as Young Stellar Objects (YSOs), Oe/Be/Ae stars, Wolf-Rayet(WR) stars, Supergiants, Planetary Nebuae(PNe), Luminous Blue Variables(LBVs), Mira stars, Flare stars, Symbiotic stars, etc. Early type ELS are identified and mainly classified them into CBe stars and Herbig Ae/Be stars (HAe/Be). A CBe star is a fast rotating B-type non-supergiant with an equatorial decretion disk (Porter & Rivinius 2003). The disk is transient in nature, which is identified through the change in Hα emission strength over a timescale of years to decades (Štefl et al. 2003). The formation of this decretion disk is known as 'Be phenomenon'.

The LAMOST one-dimensional (1D) pipeline extract and classify spectra into 4 categories (star, galaxy, QSO and unknown). From 8,813,160 spectra classified as star, 451, 695 spectra belonging to O, B and A spectral type were selected and downloaded from LAMOST DR5. Spectra with only Signal-to-Noise Ratio (SNR) greater than 10 in SDSS r-band are considered to remove noisy and unusable spectra. An automated python routine is developed to identify spectra with Hα in emission and analysed. A visually aided semi-automated template matching process using MILES spectral library has been performed to re-estimate the spectral tpes of ELS spectra. Photometric data from missions/surveys such as 2MASS, WISE, Gaia EDR3 and APASS were used to sub-classify the sample into CBe stars and HAe/Be stars. 3339 hot emission line stars have been classified into different categories *(Shridharan et al. under review).* Cross-checking these stars with the LAMOST DR6 MRS, 85 stars out of 3339 stars have medium resolution spectra available. The medium resolution

spectral data of these stars are downloaded from LAMOST DR6 database [1].

File link lists of objects with different designation ID is first downloaded. To extract FITS file in separate directories according to their respective designation ID, a shell-script was used which by entering the name of the directory that is to be created and the name of the file link list, downloads the FITS data as compressed files in the directory that is created. These files are then extracted to obtain FITS file for further analysis. The shell-script can be accessed from my GitHub repository [2].

3.2 Data Normalization

Many a times, we get a smooth wavelength-dependent signature due to the effect of the grating blaze and change in detector sensitivity over the wavelength region observed. So it is necessary to normalize the data by fitting a smooth curve through the continuum and dividing the spectrum by this fit. Normalization of an object's spectrum ensures that the continuum level is unity. Normalizing an object's flux to the continuum response is very useful while making relative measurements such as equivalent widths on a continuum, which is a strong function of wavelength.

The data is obtained in the form of FITS file from LAMOST DR6 website. The first step is to normalize the data using normalization technique. I have used *normalize_spectrum_general()* function from *laspec.normalization* module developed by Bo Zhang (Zhang et al. 2020).

3.3 Calculation of Equivalent Width

Equivalent Width is the area enclosed by the rectified continuum level and the profile of the spectral line on a plot of intensity versus wavelength of the spectra. EW measures the fraction of energy removed from the spectrum by the line regardless of the broadening intrinsic to the line or a detector with poor resolution. It is a convenient method because the shapes of spectral features can vary depending upon the configuration of the system that is producing the lines.

EW has been calculated using *measure_line_index* function of *laspec.line_index* module. The limits of integration and near approximations of the same are taken in the form of python dictionary. The output is obtained in the form of a dictionary

[1] `http://dr6.lamost.org/v2/medcas/search`
[2] `https://github.com/luciferAT02/SRFP-2021/blob/main/fits_extractor.sh`

as well. *EW['EW_int']* gives us the value of EW in terms of Å. This value is then rounded off to two decimal points.

The left and right shoulder values for calculating EW is obtained from *68-95-99.7* rule, which is applicable for all Gaussian profiles. Since Doppler profile corresponds to a Gaussian profile, this rule can yield better approximations. This rule is also known as the *empirical rule* or *three-sigma rule*, which states that in a Gaussian distribution, almost all observed data will fall within three standard deviation(σ) of their mean(μ). The rule predicts that 68% of the observed data fall under the first standard deviation ($\sigma \pm \mu$), 95% of the observed data fall under the first two standard deviations ($\sigma \pm 2\mu$) and 99.7% of the observed data fall under the first three standard deviations ($\sigma \pm 3\mu$). Using $\sigma \pm 3\mu$ as the left and right shoulder would yield better approximation of EW. The code snippet below is the python representation of the same.

Listing 1: Code snippet used for calculating FWHM

```
from laspec import line_index
mean = sum(wl)/len(wl)
var = sum((wl-mean)**2)/len(wl)
sigma = np.sqrt(var)
left = mean - 3*sigma
right = mean + 3*sigma
i = np.argmax(fl)
wav = wl[i]

line_dict_info = {'line_center': wav, 'line_range': (left,right),
'line_shoulder_left': (left-0.2,left), 'line_shoulder_right': (right,right+0.2)}

EW = line_index.measure_line_index(rwv,r[0][0],flux_err=None,
mask=None,z=None,line_info=line_dict_info,num_refit=(100, None),
filepath=None,return_type='dict',verbose=False)

EW = EW['EW_int']
```

Here,

wl and *fl* are the wavelength and flux arrays,

mean, *var* and *sigma* are mean, variance and standard deviation of the data respectively,

i is the index of the maximum value of *fl* and

wav is the wavelength value of maximum value of flux.

The value of EW is calculated by sending the line center, left shoulder and right shoulder values in a dictionary form, which here is *line_dict_info*. Using *measure_line_index* EW is calculated and is obtained in dictionary form. The value that corresponds to the key *EW['EW_int']* gives us the numerical value of EW of Hα line.

3.4 Calculation of FWHM

Doppler broadening of spectral lines of stellar sources is caused by the Doppler effect due to distribution of velocity of particles present on the stellar surface. The Doppler shift in angular frequency is given by

$$\omega = \omega_0 \left[1 \pm \frac{v}{c}\right] \tag{2}$$

The number of atoms with velocity v in the direction of the observed light is given by Boltzmann distribution as

$$n(v)dv = N\sqrt{\frac{m_0}{2\pi kT}}e^{-m_0 v^2/2kT}dv \tag{3}$$

The distribution of radiation around the central frequency is given by

$$I(\omega) = I_0 exp\left[\frac{-m_0 c^2(\omega_0 - \omega)^2}{2kT{\omega_0}^2}\right] \tag{4}$$

This is of the form of a Gaussian distribution. The width of the profile, which is also called as Doppler width, is given as

$$\Delta\lambda = \frac{\lambda}{c}\sqrt{\frac{8kTln2}{m}} \tag{5}$$

$$\frac{\Delta\lambda}{\lambda} = \frac{v}{c} \tag{6}$$

Where

$\Delta\lambda$ is the Doppler width (or) Full Width at Half Maximum value,

λ is the wavelength of light that is originally emitted by the source, and $\sqrt{\frac{8kTln2}{mc^2}} = v$ is the most probable velocity in which the particles in the star system move. In our case, we get the projected rotational velocity (vsin$i$) of the source.

The width of a spectral line at half its maximum intensity is called the Full Width at Half Maximum (FWHM) of that spectral line. FWHM depends on temperature, pressure, density and turbulence effects in stellar atmospheres.

The data is first spline-fitted using *UnivariateSpline* function of *scipy.interpolate* module. Using *spline.roots*, the roots of the interpolating function is found at half-maximum. $\Delta\lambda$ is obtained by subtracting the roots. The following code snippet shows how I have carried out the calculation of FWHM.

Listing 2: Code snippet used for calculating FWHM

```
from scipy.interpolate import UnivariateSpline
spline = UnivariateSpline(x, fl-np.max(fl)/2)
r1, r2 = spline.roots()
FWHM = r2-r1
```

Here,

x is a one-dimensional independent of the input data,

fl-np.max(fl)/2 is the flux array minus the half maximum value and

r1, r2 are the roots of the resultant spline interpolant

The variable *spline* stores the spline interpolant, which is then used find the roots at half maximum. FWHM stores the difference in the roots obtained which is the full-width at half maximum value of the $H\alpha$ line.

3.5 Calculation of Projected Rotational Velocity

After obtaining the FWHM of Hα, the projected rotational velocity is to be calculated using Doppler broadening technique. 'vsin$i$' is calculated by equation 1. We use $\Delta\lambda$ which we obtained from the previous step and $\lambda = 6562.8$ Å since we are analysing only Hα profile. The table of observation containing the Designation ID, FITS file name (FITS files obtained during different nights), EW, Projected rotational velocity and spectral type of the object is given in Table 1. The following code snippet shows the Python algorithm to calculate vsin$i$.

Listing 3: Code snippet used for calculating FWHM

```
i = np.argmax(fl)
wav = wl[i]
del_lambda = r2-r1
r1, r2 = spline.roots()
del_lambda = r2-r1
velocity = int(round(((del_lambda/wav)*c)/1000))
```

The above code calculates the value of vsin$i$ and converts it from ms^{-1} to kms^{-1}.

Table 1: Table containing corresponding EW and vsin$i$ calculated for samples taken for analysis.

Design ID	File Name	Date of Observation (MM/DD/YYYY)	Equivalent Width (Å)	vsin$i$ (km.s^{-1})	Star Classification	Spectral Type
J061948.64+225524.6	med-58086-HIP29425K201_sp06-084.fits	11/29/2017	-8.97	49	A[e]	A2V
	med-58144-HIP29425K201_sp06-084.fits	1/26/2018	-8.53	49	A[e]	A2V
	med-58114-HIP29425K201_sp06-084.fits	12/27/2017	-6.94	50	A[e]	A2V
	med-58084-HIP29425K201_sp06-084.fits	11/27/2017	-6.57	51	A[e]	A2V
	med-58186-HIP29425K201_sp06-084.fits	3/9/2018	-19.75	45	A[e]	A2V
	med-58122-HIP29425K201_sp06-084.fits	1/4/2018	-26.43	45	A[e]	A2V
	med-58088-HIP29425K201_sp06-084.fits	12/1/2017	-5.79	51	A[e]	A2V
	med-58153-HIP29425K201_sp06-084.fits	2/4/2018	-24.71	46	A[e]	A2V
J035805.42+574422.6	med-58118-HIP1893201_sp03-166.fits	3/11/2018	-19.22	58	A[e]	A0V
	med-58116-HIP1893201_sp03-166.fits	12/29/2017	-104.63	49	A[e]	A0V
J061703.73+230401.8	med-58122-HIP29425K201_sp08-088.fits	1/4/2018	-1.23	65	A[e]	A0
	med-58088-HIP29425K201_sp08-088.fits	12/1/2017	-25.45	41	A[e]	A0
	med-58086-HIP29425K201_sp08-088.fits	11/29/2017	-48.83	42	A[e]	A0
J043133.92+523039.2	med-58147-HIP2173701_sp03-092.fits	1/29/2018	-0.90	98	A[e]	A0III
J062108.89+231815.9	med-58084-HIP29425K201_sp13-063.fits	11/27/2017	-19.00	59	Ae	A1IV
	med-58088-HIP29425K201_sp13-063.fits	12/1/2017	-66.44	45	Ae	A1IV
	med-58186-HIP29425K201_sp13-063.fits	3/9/2018	-22.02	48	Ae	A1IV
	med-58086-HIP29425K201_sp13-063.fits	11/29/2017	-22.55	31	Ae	A1IV
	med-58114-HIP29425K201_sp13-063.fits	12/27/2017	-77.29	41	Ae	A1IV
	med-58122-HIP29425K201_sp13-063.fits	1/4/2018	-3.44	59	Ae	A1IV
J062115.29+225752.7	med-58122-HIP29425K201_sp06-139.fits	1/4/2018	-4.76	98	B[e]	B8III
	med-58144-HIP29425K201_sp06-139.fits	1/26/2018	-5.57	90	B[e]	B8III
	med-58065-HIP29425K201_sp06-139.fits	11/8/2017	-5.88	101	B[e]	B8III
	med-58114-HIP29425K201_sp06-139.fits	12/27/2017	-4.35	115	B[e]	B8III
	med-58088-HIP29425K201_sp06-139.fits	12/1/2017	-4.22	126	B[e]	B8III
	med-58063-HIP29425K201_sp06-139.fits	11/6/2017	-6.69	82	B[e]	B8III
	med-58086-HIP29425K201_sp06-139.fits	11/29/2017	-5.10	100	B[e]	B8III
	med-58084-HIP29425K201_sp06-139.fits	11/27/2017	-4.06	127	B[e]	B8III
	med-58186-HIP29425K201_sp06-139.fits	3/9/2018	-6.63	71	B[e]	B8III
	med-58153-HIP29425K201_sp06-139.fits	2/4/2018	-4.43	114	B[e]	B8III
J061738.64+225153.2	med-58086-HIP29425K201_sp08-075.fits	11/29/2017	-34.74	117	B[e]	B5V
	med-58186-HIP29425K201_sp08-075.fits	3/9/2018	-89.11	98	B[e]	B5V
	med-58084-HIP29425K201_sp08-075.fits	11/27/2017	-55.23	102	B[e]	B5V
	med-58153-HIP29425K201_sp08-075.fits	2/4/2018	-77.85	102	B[e]	B5V
	med-58065-HIP29425K201_sp08-075.fits	11/8/2017	-40.50	123	B[e]	B5V
	med-58114-HIP29425K201_sp08-075.fits	12/27/2017	-48.39	108	B[e]	B5V
	med-58144-HIP29425K201_sp08-075.fits	1/26/2018	-52.93	111	B[e]	B5V
	med-58122-HIP29425K201_sp08-075.fits	1/4/2018	-57.28	89	B[e]	B5V

J062018.72+230639.3	med-58186-HIP29425K201_sp06-046.fits	3/9/2018	-0.97	93	B[e]	B8
	med-58144-HIP29425K201_sp06-046.fits	1/26/2018	-0.90	97	B[e]	B8
	med-58084-HIP29425K201_sp06-046.fits	11/27/2017	-0.43	111	B[e]	B8
	med-58086-HIP29425K201_sp06-046.fits	11/29/2017	-0.64	104	B[e]	B8
	med-58122-HIP29425K201_sp06-046.fits	1/4/2018	-0.52	117	B[e]	B8
J061808.22+223701.1	med-58063-HIP29425K201_sp06-246.fits	11/6/2017	-2.47	98	B[e]	B6IV
	med-58088-HIP29425K201_sp06-246.fits	12/1/2017	-3.87	94	B[e]	B6IV
	med-58114-HIP29425K201_sp06-246.fits	12/27/2017	-4.77	89	B[e]	B6IV
	med-58086-HIP29425K201_sp06-246.fits	11/29/2017	-5.00	90	B[e]	B6IV
	med-58084-HIP29425K201_sp06-246.fits	11/27/2017	-3.73	96	B[e]	B6IV
J061149.08+224932.7	med-58186-HIP29425K201_sp06-083.fits	3/9/2018	-13.65	391	Be	B5V
	med-58063-HIP29425K201_sp06-083.fits	11/6/2017	-14.25	403	Be	B5V
	med-58144-HIP29425K201_sp06-083.fits	1/26/2018	-14.00	405	Be	B5V
	med-58084-HIP29425K201_sp06-083.fits	11/27/2017	-14.03	395	Be	B5V
	med-58065-HIP29425K201_sp06-083.fits	11/8/2017	-13.54	408	Be	B5V
	med-58153-HIP29425K201_sp06-083.fits	2/4/2018	-13.73	391	Be	B5V
	med-58088-HIP29425K201_sp06-083.fits	12/1/2017	-13.86	397	Be	B5V
	med-58122-HIP29425K201_sp06-083.fits	1/4/2018	-14.00	398	Be	B5V
	med-58114-HIP29425K201_sp06-083.fits	12/27/2017	-13.54	393	Be	B5V
	med-58086-HIP29425K201_sp06-083.fits	3/9/2018	-13.84	394	Be	B5V
J062104.61+221010.1	med-58063-HIP29425K201_sp06-106.fits	11/6/2017	-28.88	267	Be	B5V
	med-58122-HIP29425K201_sp06-106.fits	1/4/2018	-29.27	265	Be	B5V
	med-58144-HIP29425K201_sp06-106.fits	1/26/2018	-30.03	264	Be	B5V
	med-58153-HIP29425K201_sp06-106.fits	2/4/2018	-30.33	266	Be	B5V
	med-58084-HIP29425K201_sp06-106.fits	11/27/2017	-30.05	264	Be	B5V
	med-58114-HIP29425K201_sp06-106.fits	12/27/2017	-30.64	264	Be	B5V
	med-58065-HIP29425K201_sp06-106.fits	11/8/2017	-21.78	284	Be	B5V
	med-58186-HIP29425K201_sp06-106.fits	3/9/2018	-29.91	264	Be	B5V
	med-58088-HIP29425K201_sp06-106.fits	12/1/2017	-30.12	265	Be	B5V
	med-58086-HIP29425K201_sp06-106.fits	11/29/2017	-28.77	267	Be	B5V

3.6 Obtaining Representative Spectral Profiles

The relative flux (or) intensity versus wavelength graph gives us a clear insight about how much energy is carried at each wavelength. Taking wavelength in the X axis and relative flux in the Y axis, we plot the Hα profiles of the respective sources.

The representative Hα profiles of some of the objects obtained from their FITS file using python code are shown in figures 4 to 12. The python code used for analysis is available in my GitHub repository [3]

Only 30 out of 85 stars have been analysed from the list and only 11 of them had Hα profiles visible significantly.

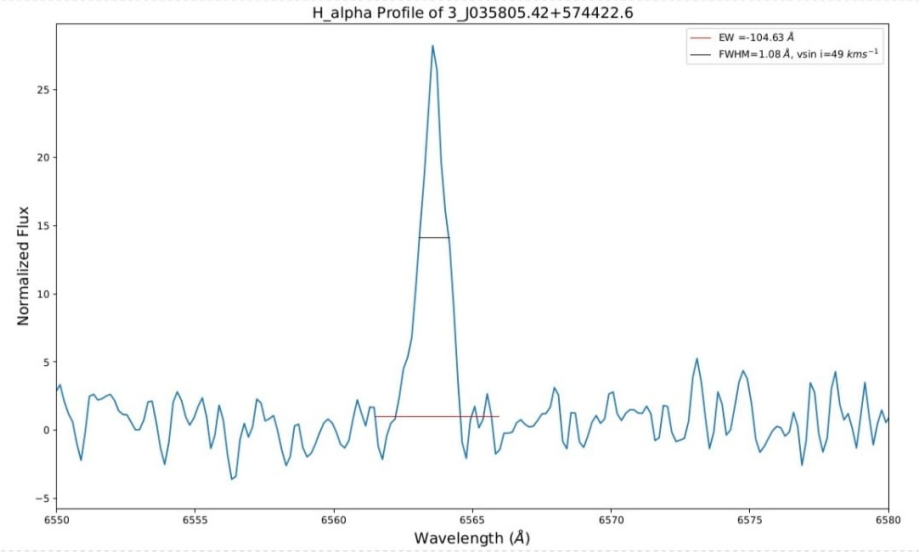

Figure 4: Hα profile of LEMC 0983 (A[e] type star)

[3] https://github.com/luciferAT02/SRFP-2021/blob/main/MRS_Final_Analysis.ipynb

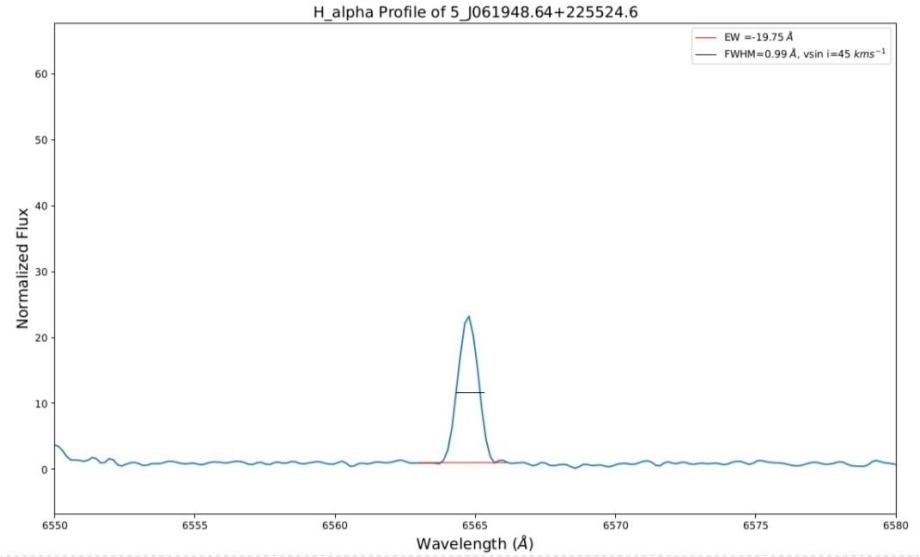

Figure 5: Hα profile of LEMC 1956 (A[e] type star)

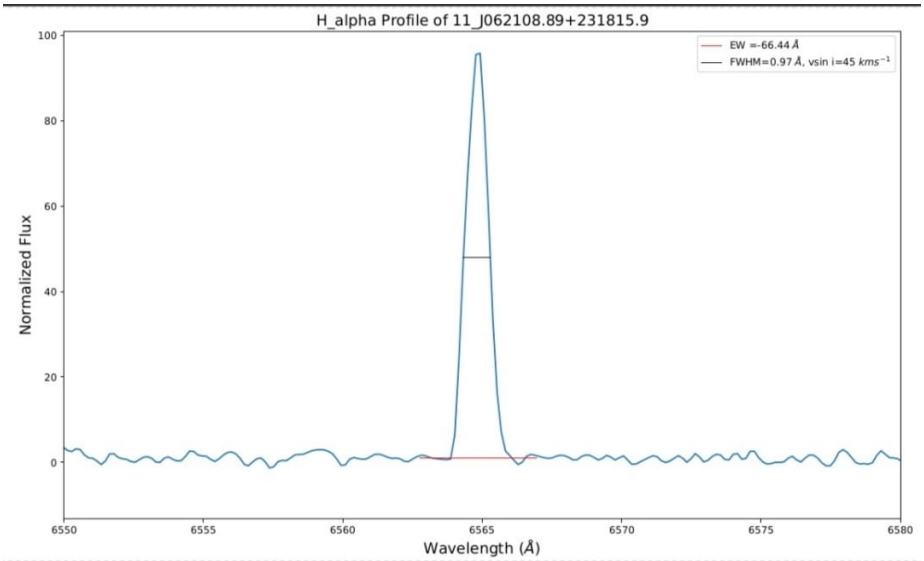

Figure 6: Hα profile of LEMC 2135 (Ae type star)

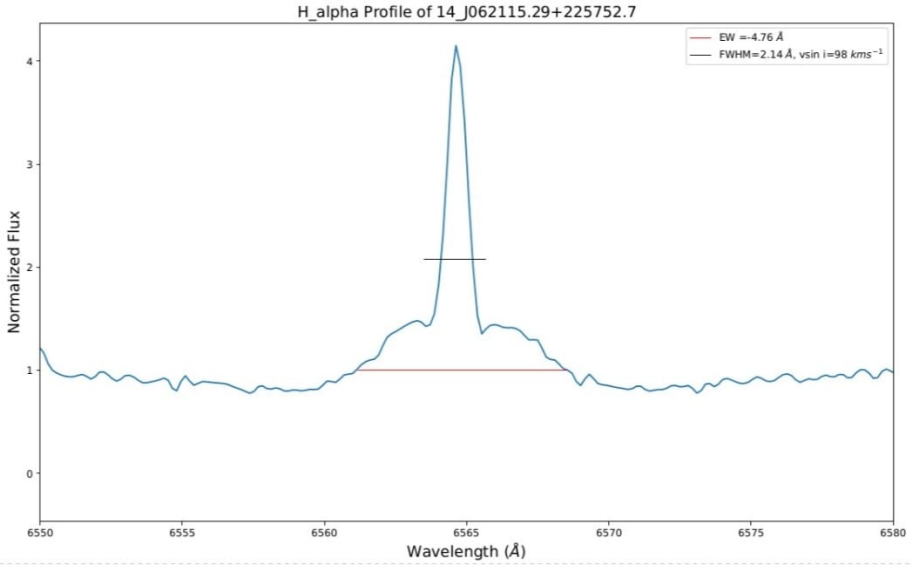

Figure 7: Hα profile of LEMC 0247 (B[e] type star)

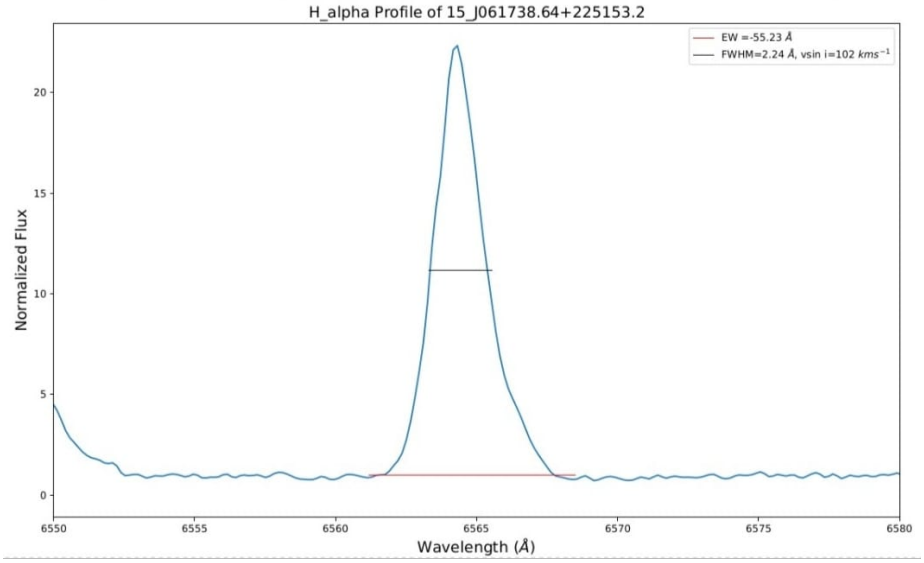

Figure 8: Hα profile of LEMC 0272 (B[e] type star)

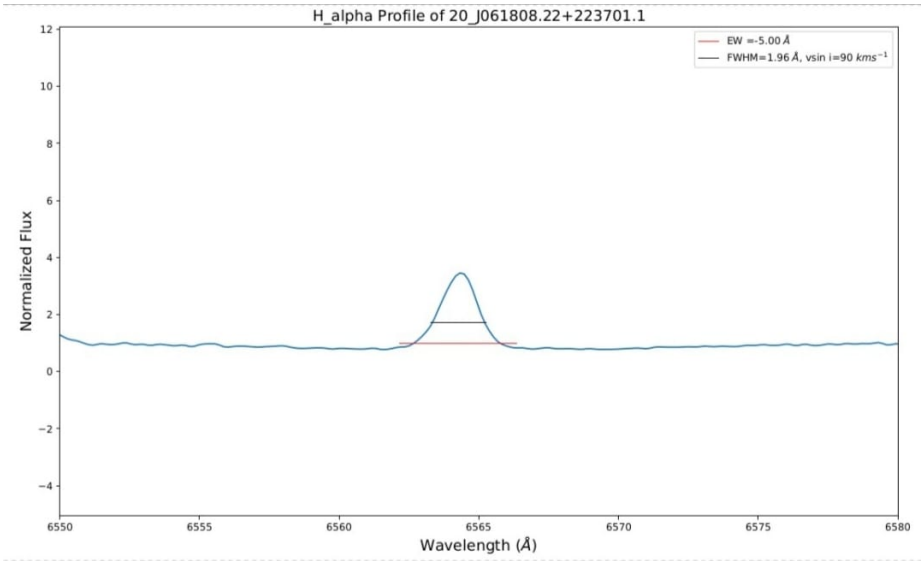

Figure 9: Hα profile of LEMC 0919 (B[e] type star)

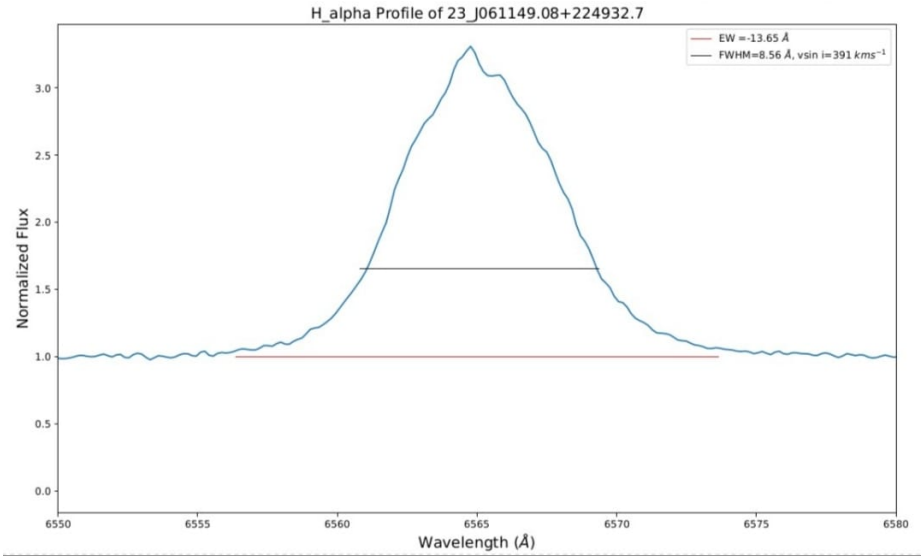

Figure 10: Hα profile of LEMC 0002 (Be type star)

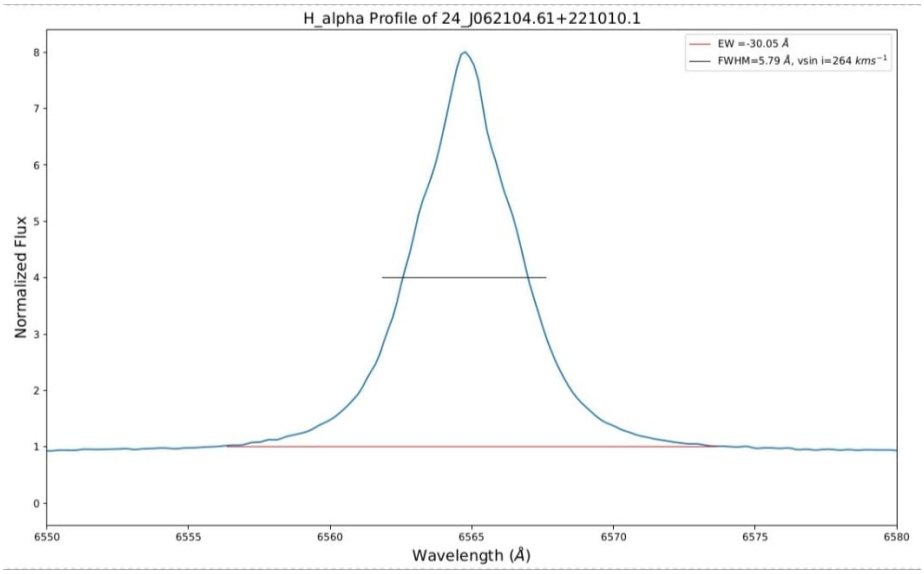

Figure 11: Hα profile of LEMC 0005 (Be type star)

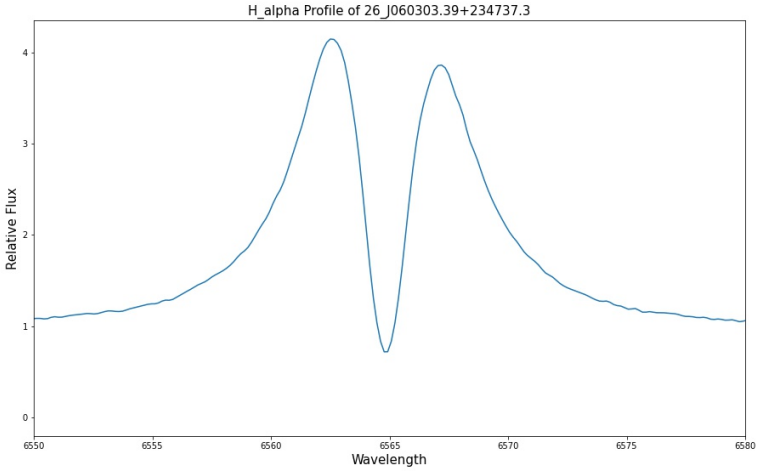

Figure 12: Hα profile of LEMC 0009 (Be type star). A double peak was observed.

4 Result and Discussion

Out of 30 samples taken for observation, most of the profiles had single peak above continuum. Some Be star samples showed double peaks as well (Figure 12). Comparing Figure 11 and Figure 12 with the others, we can conclude that Be type stars show stronger effects of Doppler broadening compared to other samples.

Be stars are hot massive type stars, which are one among the foremost important stellar groups being important sources of UV photons. A Be star is a special class of massive B-type main sequence star surrounded by a geometrically thin, equatorial, gaseous, decretion disk that orbits the star in near Keplerian rotation. The working definition of a classical Be star was given as "a non-supergiant B star whose spectrum has, or had at some time, one or more Balmer lines in emission". The presence of circumstellar disk results in prominent Balmer emission lines. The rotational motion of circumstellar disk may have given rise to a strong Doppler profile. The double peak observed might be possible because of viewing angle or the source can be a pole-on star.

The formation of disk in Be type stars is known as Be phenomenon. This is also observed in late O- and early A- type stars. Classical Ae stars can be considered as late-type analogs to CBe stars. Late-type Be and early-type Ae stars are relatively at ease in forming a Keplerian disc because of their closer proximity to the critical rotation speed.

A[e] and B[e] type stars are typical A-type and B-type stars with distinctive forbidden neutral or low ionization emission lines in its spectrum. A forbidden line is a spectral line associated with emission of photons by atomic nuclei, atoms or molecules, which undergo a transition that is not allowed by a particular selection rule but is allowed if the approximation associated with that rule is not made.

A box plot of star classification between projected rotational velocity and star classification versus equivalent width has been obtained from the results obtained from the python code which are show below. Box plot is a way of displaying the distribution of data based on a five-number summary (first quartile, median, third quartile and the maximum). It is similar to the empirical rule - 50% of data lie between Q1 and Q3, 99.7% of the data lie within Q1-1.5 x IQR and Q3+1.5 x IQR, where IQR is the interquartile range, the middle line is the median and Q1 and Q3 are the first and third quartiles. Points lying outside the whiskers are called outliers. The correction term required in Doppler broadening has not been considered anywhere. This could have introduced error in the value of projected velocities calculated.

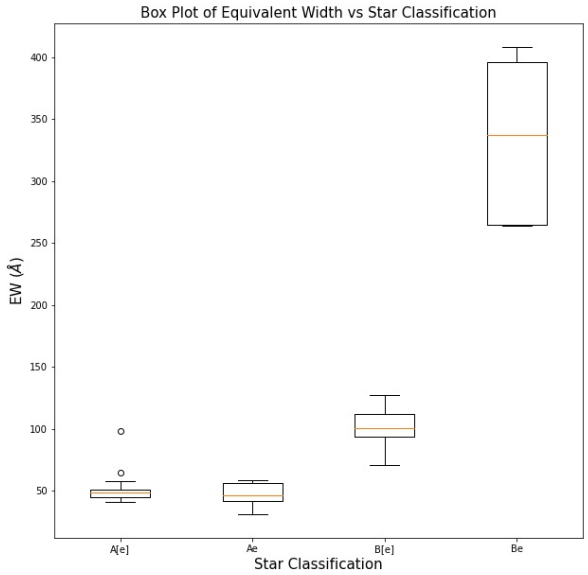

Figure 13: Box plot of '$v \sin i$' versus star classification with error bars as standard deviation of the values of '$v \sin i$'.

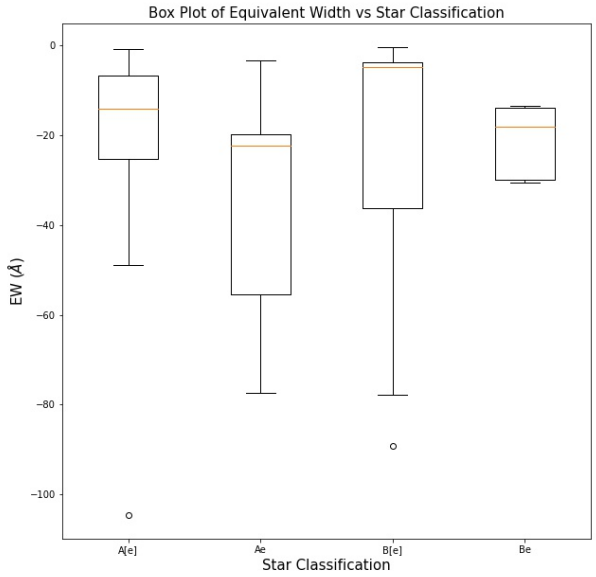

Figure 14: Box plot of equivalent width of Hα versus star classification with error bars as standard deviation of the values of EW.

From Table 1 and Figure 13, it is evident that Be type stars rotate the fastest showing more variability in their values, followed by B[e], A[e] and Ae type stars. From Figure 14 we can see that range of EW values of Ae type star seems to be the greatest followed by B[e], Be and A[e] type stars, which we can see from the representative Hα profiles.

5 Conclusion

- Out of the 85 stars from LAMOST DR5 that have medium resolution spectra available in LAMOST DR6, the Hα profiles of 30 star samples were analysed and their respective equivalent widths and projected rotational velocities were estimated using python code.
- We identified 2 different types of Hα profile in our sample namely single peaked emission (e) and double peaked emission (dpe). Double peaked emission was observed in Be type star samples. The projected rotational velocities of samples with single peaked emission were estimated by spline fitting the data.
- In A[e] type stars, 92.86% of the data show value of EW below -50Å and the remaining 7.14% of the data have EW value above -100Å. In case of vsin$i$, 57.14% of the data lie between 40-50kms^{-1}, 28.57% of the data lie between 50-60kms^{-1} and 14.29% of the data lie between 60-100kms^{-1}
- In Ae type stars, 66.67% of the data show value of EW within -30Å and vsin$i$ value between 30-50kms^{-1}. Around 33.33% of the data show value of EW between -60Å to -80Å and the value of vsin$i$ around 59kms^{-1}.
- In B[e] type stars, 71.43% of the data show value of EW below -10Å and 28.57% of the data between -30Åto -90Å. In case of vsin$i$, 50% of the data lie between 70-90kms^{-1}, 28.57% of the data in the range 90-100kms^{-1} and 21.43% of the data in the range of 100-130kms^{-1}.
- In Be type stars, 50% of the data show value of EW around -13Å to -14Å and the other 50% of the data around -28Å to -30Å. In case of vsin$i$, 50% of data lie in the range 390-410kms^{-1} and the other 50% of the data around 264kms^{-1}.
- Figure 14 suggest that Ae type stars possess the highest EW followed by Be, A[e] and B[e] type stars. From figure **??**, we can conclude that Be type stars rotate the fastest followed by B[e], A[e] and Ae type stars.

6 Future Scope

- It has to be noted that the present study only analyzed 30 stars from data. This analysis can be extended further to the remaining 85 stars and their projected rotational velocity can be estimated.
- As we include more stars in our study as mentioned above, one can compare the distribution of rotational velocity with respect to different spectral subtypes.
- Taking into consideration the uncertainty term arising due to Doppler broadening could help in arriving at a conclusion about the rotation of the samples with more certainty.
- Instead of using *UnivariateSpline* to fit the data, we could use Gaussian fit to get more precise results as Doppler broadening originally corresponds to a Gaussian profile. Change in values of FWHM will correspond to change in 'vsin$i$'.This could also help with estimating rotational velocities of objects that show double peaks in their Hα profiles.
- The present analysis can also be extended to HeI lines to understand the stellar rotation as they originate from the photosphere. Taking Helium lines into consideration along with Hα lines, we can perform a comparative study on the rotational differences between the disc and star system. More certain conclusions can be made on the projected rotational velocity, critical or break-up velocity v_c and the decretion disk surrounding the Be star samples as well.
- As the data comprise of different types of emission-line stars, an evolutionary comparison in rotational velocity between pre-main-sequence and main-sequence stars can be obtained using additional samples.
- Making use of the multi-epochs of observation, V/R variability studies can be performed and changes in rotational velocity during these phases can also be examined.

References

[1] Carroll, Bradley W., and Dale A. Ostlie. An introduction to modern astrophysics. Cambridge University Press, 2017.

[2] Kogure, Tomokazu, and Kam-Ching Leung. The astrophysics of emission-line stars. Vol. 342. Springer Science & Business Media, 2010.

[3] Collins, G.W., 1989. The fundamentals of stellar astrophysics. New York, WH Freeman and Co., 1989, 512 p.

[4] Walker, R., Trypsteen, M. F. M. (2017). Spectroscopy for Amateur Astronomers: Recording, Processing, Analysis and Interpretation. United Kingdom: Cambridge University Press.

[5] Bhat, S.S., Paul, K.T., Subramaniam, A. and Mathew, B., 2016. Spectroscopic study of Be-shell stars: 4 Her and 88 Her. Research in Astronomy and Astrophysics, 16(5), p.076.

[6] Anusha, R., Mathew, B., Shridharan, B., Arun, R., Nidhi, S., Banerjee, G., Kartha, S.S., Paul, K.T. and Bhattacharyya, S., 2021. Identification of new classical Ae stars in the Galaxy using LAMOST DR5. Monthly Notices of the Royal Astronomical Society, 501(4), pp.5927-5937.

[7] Porter J. M., Rivinius T., 2003, PASP, 115, 1153.

[8] Stefl S., Baade D., Rivinius T., Stahl O., Budovi ˇ cov ˇ a A., Kaufer A., Maintz M., 2003, ´ A&A, 411, 167.

[9] Carciofi, A.C., 2010. The circumstellar discs of Be stars. Proceedings of the International Astronomical Union, 6(S272), pp.325-336.

[10] Aret, A., Kraus, M. and Šlechta, M., 2016. Spectroscopic survey of emission-line stars–I. B [e] stars. Monthly Notices of the Royal Astronomical Society, 456(2), pp.1424-1437.

[11] Townsend, R.H., Owocki, S.P. and Howarth, I.D., 2004. Be-star rotation: how close to critical?. Monthly Notices of the Royal Astronomical Society, 350(1), pp.189-195.

[12] Hou, W., Luo, A.L., Hu, J.Y., Yang, H.F., Du, C.D., Liu, C., Lee, C.D., Lin, C.C., Wang, Y.F., Zhang, Y. and Cao, Z.H., 2016. A catalog of early-type emission-

line stars and Hα line profiles from LAMOST DR2. Research in Astronomy and Astrophysics, 16(9), p.138.

[13] Zhang, B., "Self-consistent Stellar Radial Velocities from LAMOST Medium-Resolution Survey (MRS) DR7", arXiv e-prints, 2021.

[14] Zhang, B., Liu, C., and Deng, L.-C., "Deriving the Stellar Labels of LAMOST Spectra with the Stellar LAbel Machine (SLAM)", The Astrophysical Journal Supplement Series, vol. 246, no. 1, 2020. doi:10.3847/1538-4365/ab55ef.

[15] http://www.lamost.org/public/?locale=en

[16] https://aas.aanda.org/articles/aas/full/1997/11/ds1267/node3.html

[17] https://cefrc.princeton.edu/sites/cefrc/files/Files/2013%20Lecture%20Notes/Hanson/pLecture6.pdf

[18] http://hyperphysics.phy-astr.gsu.edu/hbase/Atomic/broaden.html

[19] http://www-star.st-and.ac.uk/~kw25/teaching/nebulae/lecture08_linewidths.pdf